Sensors and Modeling in Materials Processing: Techniques and Applications, S. Viswanathan, R.G. Reddy, and J.C. Malas, eds., The Minerals, Metals, & Materials Society, Warrendale, PA., 1997. pp. 117-142.

EFFECT OF TRANSVERSE DEPRESSIONS AND OSCILLATION MARKS ON HEAT TRANSFER IN THE CONTINUOUS CASTING MOLD

B. G. Thomas, D. Lui, and B. Ho

Department of Mechanical and Industrial Engineering
University of Illinois at Urbana-Champaign
1206 West Green Street
Urbana, IL 61801

Abstract

Results from mathematical models and plant experiments are combined to quantify the effect of transverse depressions and oscillation marks on heat transfer in the continuous casting mold. A heat transfer model has been developed to calculate transient heat conduction within the solidifying steel, coupled with the steady-state heat conduction with the continuous casting mold wall. The model features a detailed treatment of the interfacial gap between the shell and mold, including mass and momentum balances on the solid and liquid powder layers. The model predicts the solidified shell thickness down the mold, temperature in the mold and shell, thickness of the resolidified and liquid powder layers, heat flux distribution down the mold, mold water temperature rise, ideal taper of the mold walls, and other related phenomena. The important effect of non-uniform distribution of superheat is incorporated using the results from previous 3-D turbulent fluid flow calculations within the liquid cavity. Results from plant experiments confirm that transverse surface depressions and oscillation marks form at the meniscus and move down the mold. Measurements of mold thermocouple temperatures and breakout shell thickness were used to calibrate the models. The results indicate that the surface depressions and oscillation marks are filled with mold flux, but still have a significant effect on decreasing heat transfer. The predicted mold temperature fluctuations are consistent with measurements. If the depressions become filled with air, their effect is greatly increased. These results should be useful in the difficult task of interpreting transient mold thermocouple signals for on-line quality monitoring.

Introduction

Many different types of intermittent surface defects on steel slabs arise during initial solidification in the mold of the continuous casting machine. These defects include deep oscillation marks, surface depressions, and cracks. They may lead to quality problems, such as slivers, in the final rolled product. In severe cases, breakouts may occur, where liquid steel bursts through a thin section of the shell and drains over the casting machine below the mold.

It is recognized that on-line monitoring of temperature fluctuations in the mold walls using thermocouple signals should be useful in identifying the presence of such surface defects. [1] This is already used for the prediction and prevention of breakouts. [2]

If better understood, patterns in the temperature signals might also be used to predict surface quality problems, which would ease the burden of surface inspection. Developing algorithms to match thermocouple signals with these problems is a difficult task, however. A critical step is understanding the relationship between thermocouple signals and the condition of the mold / metal interface, including the shape of the solid shell surface. This work attempts to contribute towards this understanding by developing mathematical models of interface heat transfer, and applying them to quantify the effect of transverse surface depressions and oscillation marks on heat flow in the continuous casting mold.

Description of Phenomena

Figure 1 illustrates the solidifying steel shell moving down the mold during the initial stages of solidification in a continuous casting machine with mold flux. To help prevent sticking between the shell and mold, and to entrain liquid mold flux into the interfacial gap, the mold is oscillated vertically throughout casting. Each oscillation cycle creates a depression in the solidifying shell at the meniscus, called an "oscillation mark". The cause of these depressions has been the subject of much study. They are believed to form due to a variety of different mechanisms, which may act in combination. These include freezing and overflow of the meniscus, [3] thermal stresses in the solidifying shell [4] and bending of the weak shell by the interaction between pressure in the liquid flux layers and ferrostatic pressure. [3]

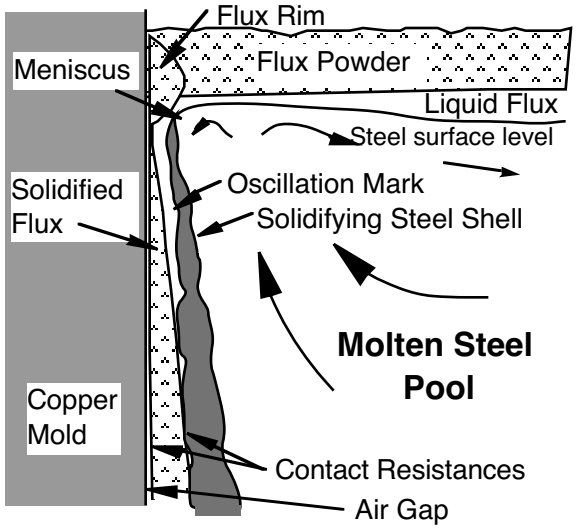

Figure 1 - Schematic of initial solidification near meniscus

During stable casting, these oscillation marks appear as shallow, equally-spaced horizontal depressions on the surface of final as-cast steel slabs and blooms. If the metal level is unstable due to turbulence or waves on the top surface, the oscillation marks will become nonuniform and the solid surface may contain other more serious defects, such as ripples or deep depressions.

As the strand moves down the mold, heat transfer is controlled by heat conduction across the interfacial gap between the mold and shell,. The gap contains layers of solid and liquid flux and possibly air. Heat transfer is reduced locally beneath surface depressions because the gap is larger there. If the gap becomes filled with air, its lower thermal conductivity further reduces heat flow. The reduction in heat flow results in a thinner solidified shell locally. In addition, as each depression passes by a given point on the mold wall, the temporary drop in the rate of heat transfer causes a temporary drop in the mold wall temperature. Analysis of these mold wall temperatures should enable prediction of the surface defects that produced them, if the relationship can be quantified. In addition, simultaneous examination of the temperatures and depressions can be used to further understand the nature of the gap.

Previous Work

Experimental Studies

Previous work has presumed a relationship between oscillation mark depth and mold heat transfer. Oscillation marks are believed to increase the effective gap, reduce heat transfer, and retard shell growth. [5-7] This relationship has been used to explain many phenomena in continuous casting. For example, Mahapatra et al. [5] observed lower heat transfer on the inside radius and at low casting speed. This was attributed to deeper oscillation marks for these conditions.

Other experimental works with both oil lubricated billet molds [8-10] and flux-lubricated slab molds [11, 12] have established a minimum in heat flux for “middle-carbon” steels with carbon contents of 0.10 - 0.12%C. Depending on the lubricant used, these steels have a mold heat flux about 15-30% lower than steels with above 0.25%C. [8, 9, 11, 12] This drop in heat transfer has been associated with the deeper oscillation marks that have been observed in these steels by several researchers. Tiedje and Langer [13] reported the deepest oscillation marks to appear in 0.07 and 0.13 %C steels. In flux-lubricated steels, Cramb and Mannion [14] found the deepest oscillation marks in 0.10% C steel. Mahapatra et al. [5] reported that 0.04 - 0.09%C steels had 0.5 - 1.25 mm deep oscillation marks, compared with only 0.35 - 0.8 mm depths for higher carbon steels.

To understand mold heat transfer and interpret mold thermocouple signals, this relationship between oscillation mark / depressions and heat transfer needs to be quantified. Little previous work has been done.

Mathematical Models

Many mathematical models have been developed of the continuous casting process, which are partly summarized in a previous literature review. [15] Many of these models are very sophisticated (even requiring supercomputers to run) so are infeasible for use in an operating environment. Of the remaining models which consider the mold, most simulate either solidification of the shell, or heat conduction through the mold. There is usually a simplified treatment of the interfacial gap, despite its known importance. A few models have considered more detailed treatment of the powder layers in the gap. [16] These models have generally oversimplified the shell and mold. To study practical problems, such as the effect of shell surface depressions on heat transfer in an operating caster, two new models were developed and applied in this work.

Bloom surface defect measurements

An example of the mold temperature signals that were recorded by thermocouples embedded in the copper walls of a continuous casting mold is shown in Figure 2. These three particular signal portions were recorded from a bloom caster at BHP RBPD in Newcastle, Australia for conditions given in Table I. [17] They record the passage of a particular deep transverse depression, as it moved down the mold.

The horizontal axis indicates the time since the depression was created at the meniscus. Knowing the casting speed (0.5 m min^{-1}), and metal level (-125mm), this axis is also related to distance below the top of the mold.

Figure 2 quantifies how a surface depression causes a drop in the recorded mold temperature as it passes by each mold thermocouple. The time when each thermocouple reaches its minimum temperature coincides exactly with the time required for that portion of the shell to travel to that thermocouple.

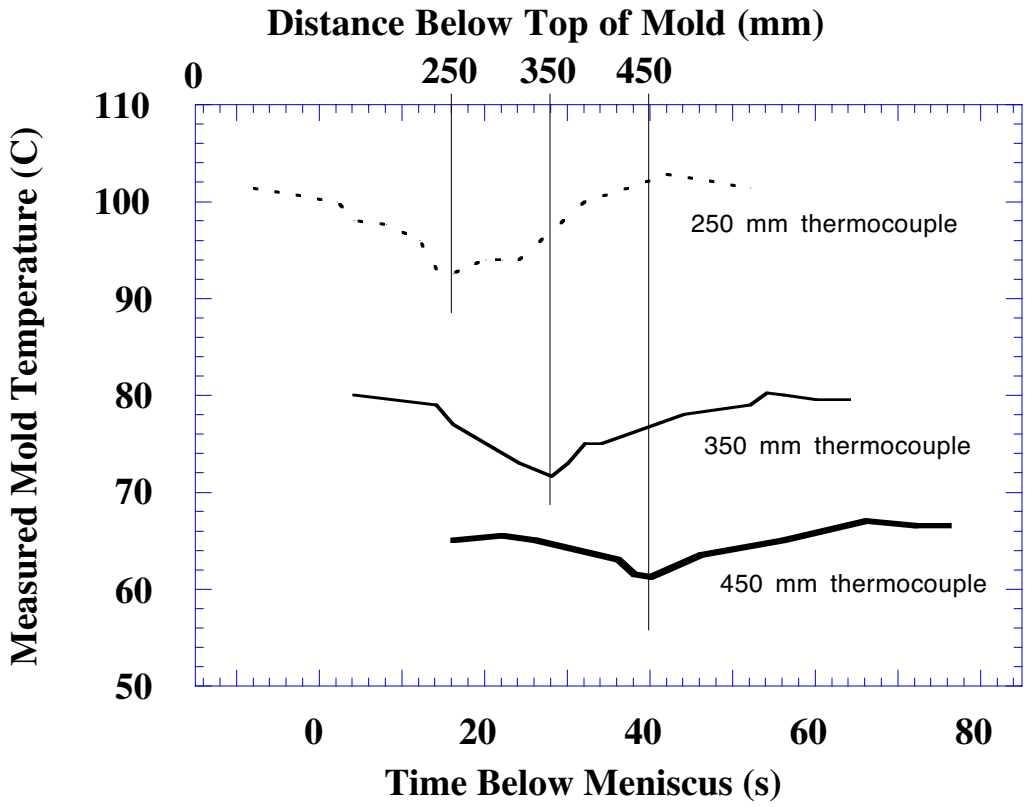

Figure 2 - Mold thermocouple signals (RBPD bloom caster).

Note that the shape of the temperature profile remains similar, also. Indeed, the distinctive pattern of the thermocouple signals for about 15 minutes is what enabled an exact match to be made between time and position on the final bloom. [17] A series of 14 severe transverse surface depressions on the surface of two blooms matched exactly with time-shifted drops in mold temperature as those defects passed by each thermocouple. By extrapolating back to the meniscus metal level, it was possible to determine the time that each defect was formed. This time corresponded exactly with 14 peaks in mold level that were recorded during that time period.

In addition to illustrating the correspondence between surface depressions and thermocouple signals, this work demonstrated that the depressions were formed at the meniscus due to gradual changes in metal level. [17] The defects were spaced about 600 mm apart, and were experienced on the first blooms cast after a startup or grade change. Their cause may be related to excessive buildup of the solidified flux rim at the meniscus with certain startup powders, combined with mold level fluctuations, possibly due to periodic bulging below the mold. Further details and solutions to the problem are discussed elsewhere. [17]

The severity of the temperature drop recorded by mold thermocouples depends on the nature of the interfacial gap and the severity of the defect. The depressions in this work were about 200 mm in length, with a maximum depth of about 2 mm. Although each depression extended around the entire bloom perimeter, measurements were made on the narrow face, where there were no rolls to deform the surface.

Knowing both the temperature drops and the dimensions of the defect, it was possible to calibrate mathematical models, described later in this work, to increase understanding of the interfacial gap. The results determined that the gap must have been filled with mold flux while in the mold. The same methodology is employed in the present work to understand the nature of the interfacial gap and heat transfer losses resulting from oscillation marks.

Breakout shell measurements

Measurements were performed on a breakout shell to quantify the relationship between oscillation mark depth and shell thickness with distance below the meniscus. The breakout shell was obtained from a slab cast at LTV Steel under conditions given in Table I. Measurements were made down the wide-face centerline (mid-wide face), the narrow-face centerline (mid-narrow face), and the wide face outer radius at a distance of 75 mm from the corner (off-corner wide face) opposite the corner where the breakout occurred.

Oscillation mark depths were measured along all three of these locations, as shown in Figure 3. The maximum distance was measured between each oscillation mark and a flat surface (15 mm long) that was placed against the shell. Measurements were made using a profilometer gauge and photocopy enlargements of silicone rubber impressions of specific longitudinal sections of shell. The estimated accuracy is within ±0.02 mm.

The corresponding shell thickness profiles are shown in Figure 4. Each data point is averaged from 3 different transverse measurements at 12.7 mm intervals down each shell. Replicate tests determined the accuracy of these measurements to be ± 0.11 mm.

The distance between oscillation marks, L_{pitch}, averages about 10.5 mm, which is close to the ratio of the casting speed (1.016 m min^{-1}) and the oscillation frequency (85 cycles per min), as expected.

Oscillation Mark Depth

Based on Figure 3, there is no relation between oscillation mark depth and distance down the mold, beyond the first 100 mm. There is a slight trend of increasing depth with distance over the first 100 mm below the meniscus. These measurements confirm that oscillation marks form at the meniscus and do not change their shape beyond the first 100 mm.

Oscillation mark depth was deepest and most variable along the off-corner wide face location. Here, the average depth was 0.33 ± 0.17 mm, with an average width of 3.78 mm. Average depth was only 0.31 ± 0.09 mm along the wideface and 0.22 ±0.10 mm along the narrowface. This is likely explained the nature of surface flow near the meniscus, which is most chaotic at the offcorner position. Here, the standing wave height fluctuates greatly and interrupts the uniform flow of liquid flux feeding into the gap at the meniscus, so creates deeper, more variable marks.

A reasonable correlation exists between oscillation mark depth and width, as deeper marks generally tended to be wider. This is shown in Figure 5, which presents several example oscillation mark shapes. However, the deepest oscillation marks were actually surface depressions, which were irregular in shape with large widths sometimes exceeding 10 mm. These wide, irregular marks, produced the most obvious locally thin regions in the shells. Their profiles are presented later.

Shell thickness

The shell thickness is generally greatest along the midwide face, where superheat dissipation is a minimum. This is shown in Figure 4. Shell growth down the narrow face and off-corner regions is slower due to the larger superheat, perhaps combined with decreased interfacial heat transfer due to larger air gap(s). Growth along the narrowface is slowest, particularly near the point of jet impingement between 300 and 1000 mm below the meniscus, where most of the superheat is dissipated on this shell. Oscillation marks are clearly less important than these other factors, as their shallower depth on the narrow face would tend to make the shell thicker.

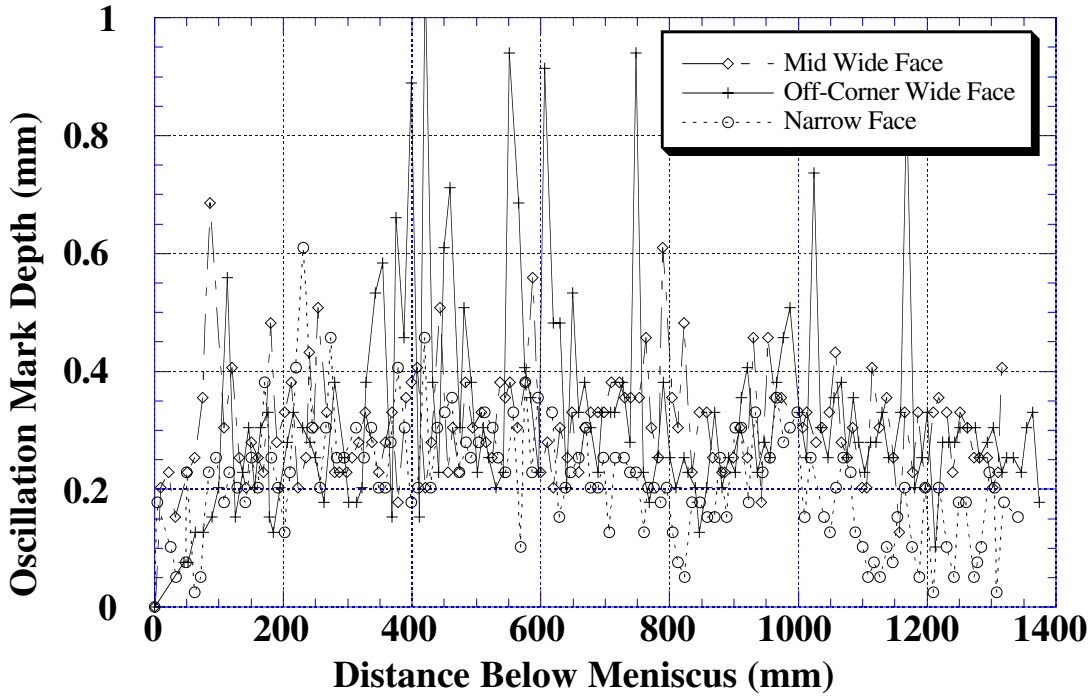

Figure 3 - Oscillation mark depth measured down break-out shells.

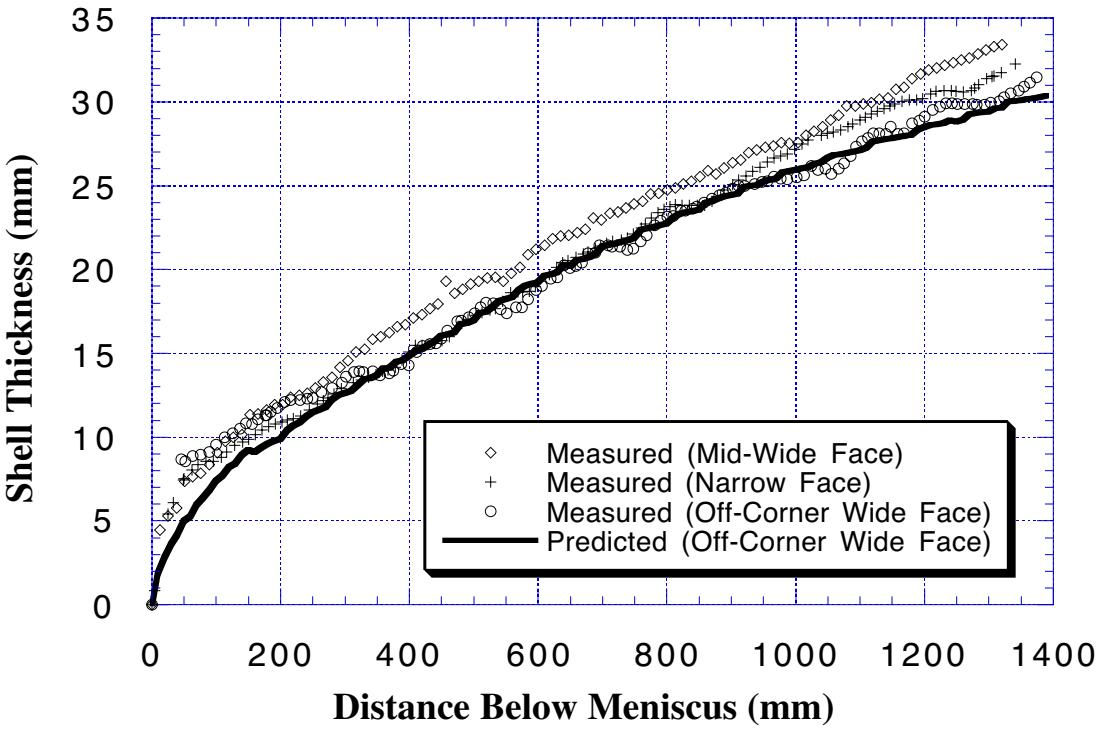

Figure 4 - Comparison of predicted shell thickness down the mold with breakout shell measurements.

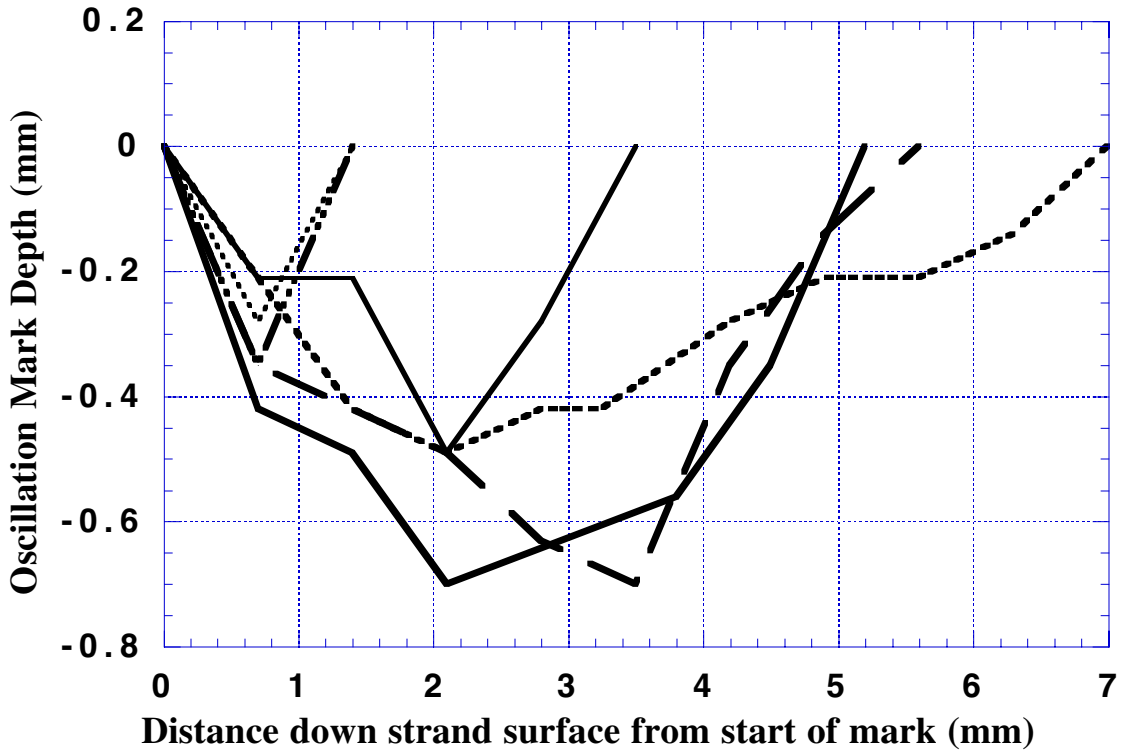

Figure 5 - Profiles of individual oscillation marks (located 320-380 mm below meniscus on wideface off-corner breakout shell)

Relationship between mark depth and shell thickness

To explore the effect of oscillation mark depth on shell thickness, the shell thickness data, d_s, was normalized according to the time spent in the mold, assuming a simple square root relationship. The normalized variable, called the solidification constant, K, is $d_s\sqrt{V_c/z}$. Typical results are shown in Figure 6. Examination of K at different distances down the mold, z, reveals that the shell thickness grows faster at first than predicted by this relation, as K is large. It drops to a minimum from $150 < z < 400$ mm, before increasing with distance down the rest of the mold. This variation is consistent with the effect of superheat.

The effect of oscillation mark depth on shell growth is slight, but consistent. Deeper oscillation marks decrease shell growth rate (represented by K) for every region of every breakout shell examined. [18] The trend is strongest high in the mold, where gap heat conduction has the strongest influence on heat transfer, (and consequently shell thickness). Lower down the mold, the variability almost obscures the trend, unless the marks are very deep.

The results also revealed that groups of adjacent oscillation marks work together to affect heat transfer. Thus, in constructing Figure 6, each x data point was obtained by averaging the depths of the oscillation mark and its two neighbors (3 points). This greatly improved the correlation between increasing oscillation mark depth and decreasing shell growth rate.

In general, deeper oscillation marks had a thinner corresponding shell thickness. However, the very wide, irregular marks had the thinnest shells, even though they were relatively shallow. This is because the region of reduced heat transfer extends over a longer distance. This indicates that oscillation mark area may be a better measure of the effect of oscillation marks on heat transfer than just their depth.

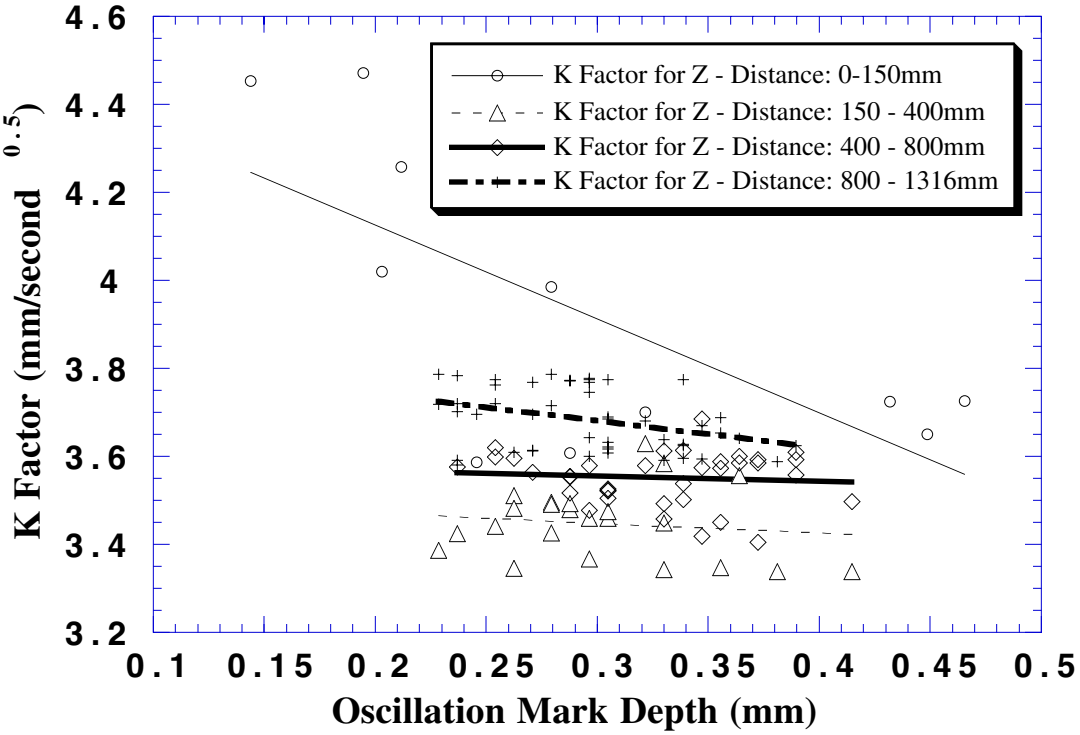

Figure 6 - Effect of Oscillation Mark Depth on Shell Growth Along Various Regions of the Mid-Wideface Breakout Shell for 3 Oscillation Marks

CON1D Model Description

A heat transfer model, CON1D, [19] has been developed to predict the time-averaged temperature distribution in the shell, mold, and gap. It consists of 2-D steady-state heat conduction within the mold, coupled with 1-D transient heat flow through the solidifying steel shell, as it moves down through the mold. The model simulates axial behavior down a chosen position on the mold perimeter. Mid-wideface and mid-narrow face simulations can thus be conducted separately. The model features a detailed treatment of the interface, which controls heat flow as shown in Figure 7. A brief description of the model is given here, as further details are provided elsewhere. [19, 20]

Heat Conduction in the Solidifying Steel Shell

Temperature in the thin solidifying steel shell is governed by the 1-D transient heat conduction equation, which includes grade- and temperature-dependent thermal properties:

$$\rho C_p^* \frac{\partial T}{\partial t} = k \frac{\partial^2 T}{\partial x^2} + \frac{\partial k}{\partial T} \left(\frac{\partial T}{\partial x} \right)^2 \qquad (1)$$

where $C_p^* = C_p + \frac{\Delta H_L}{T_{liq} - T_{sol}}$

This equation assumes that axial heat conduction is negligible, (due to the large advection component) and that latent heat is evolved linearly between the solidus and liquidus temperatures. The simulation domain is a slice through the liquid steel and solid shell pictured in Figure 8 together with the boundary conditions. The boundary condition on the external surface of the shell imposes the heat flux lost to the interfacial gap, q_{int}, which depends on the behavior of the flux layer, described in detail later. The internal solid / liquid steel interface incorporates the "superheat flux" delivered from the turbulent liquid pool, described next.

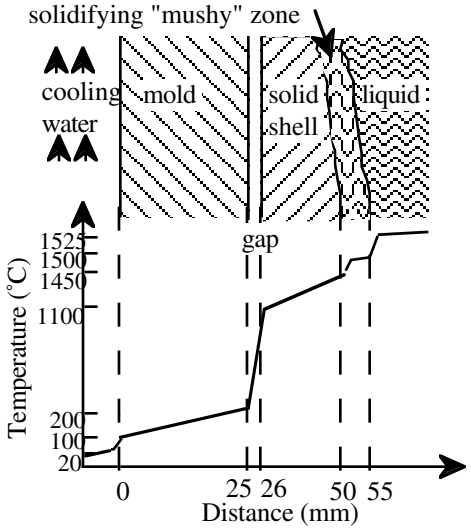

Figure 7 - Typical temperature distribution in slab casting showing importance of interface

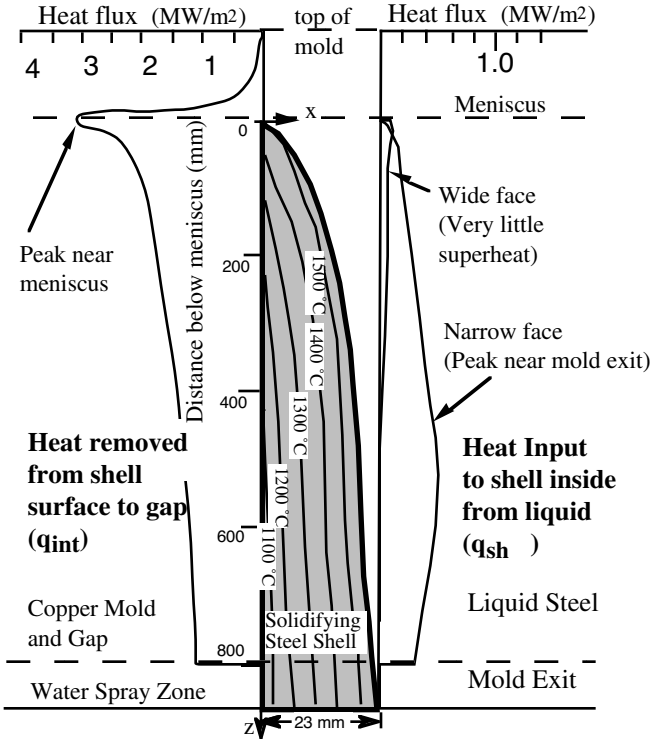

Figure 8 - Typical isotherms and boundary conditions calculated on shell solidifying in mold

Superheat Delivery

Before it solidifies, the steel must first cool from its initial pour temperature to the liquidus temperature. Due to turbulent convection in the liquid pool, the "superheat" contained in this liquid is not distributed uniformly. A small database of results from a 3-D fluid flow model [21] is used to determine the heat flux delivered to the solid / liquid interface due to the superheat dissipation, as a function of distance below the meniscus, q_{sh}. Examples of this function are included in Figure 8, which represents results for a typical bifurcated, downward-directing nozzle. The initial condition on the liquid steel at the meniscus is then simply the liquidus temperature.

This superheat function incorporates the variation in superheat flux according to the superheat temperature difference, ΔT_{sh}, casting speed, V_c, and nozzle configuration. The influence of this function is insignificant to shell growth on most of the wide face, where superheat flux is small and contact with the mold is good.

Heat Conduction in the Mold

Two dimensional, steady state temperatures within a rectangular vertical section through the upper portion of the mold are calculated by solving:

$$k_m \left(\frac{\partial^2 T}{\partial x^2} + \frac{\partial^2 T}{\partial y^2} \right) = 0 \qquad (2)$$

Below the meniscus region, (generally chosen to extend from the top of the mold to 50 mm below the meniscus), heat flow is almost one dimensional. Heat flow through the mold is then characterized simply by:

$$T_{hotc} = T_{water} + q_{int} \left(\frac{1.}{h_{water}} + \frac{d_m}{k_m} \right) \quad (3)$$

The calculation requires, as boundary conditions, the heat flux across the interface, q_{int}, the initial cooling water temperature, T_{water}, and the effective heat transfer coefficient to the water, h_{water}.

Convection to the Cooling Water

The effective heat transfer coefficient between the cooling water and the cold face ("water-side") of the mold, h_{water}, is calculated including a possible resistance due to scale deposits on the surface of the cooling water channels:

$$h_{water} = \frac{1}{\frac{d_{scale}}{k_{scale}} + \frac{1}{h_{fin}}} \quad (4)$$

To account for the complex nature of heat flow in the undiscretized width direction, the heat transfer coefficient between the mold cold face and the cooling water, h_{fin}, treats the sides of the water channels as heat-transfer fins.

$$h_{fin} = \frac{h_w \, w_{ch}}{L_{ch}} + \frac{\sqrt{2h_w \, k_m (L_{ch} - w_{ch})}}{L_{ch}} \tanh \sqrt{\frac{2h_w \, d_m}{k_m (L_{ch} - w_{ch})}} \quad (5)$$

where L_{ch}, w_{ch}, d_m, d_{ch} are geometry parameters shown in Figure 9 and k_m is the mold (copper) thermal conductivity. The heat transfer coefficient between the water and the sides of the water channel, h_w, is calculated assuming turbulent flow through an equivalent-diameter pipe. [22]

This equation assumes that the base of the water slot has constant temperature, so is most accurate for closely-spaced slots. The presence of the water slots can either enhance or diminish the heat transfer relative to a mold with constant thickness, d_m. Deep, closely-spaced slots augment the heat transfer coefficient, (h_{fin} larger than h_w) while shallow, widely-spaced slots inhibit heat transfer. In most molds, h_{fin} and h_w are very close.

Heat Transfer Across the Interfacial Gap

Heat transfer across the interfacial gap governs the heat flux leaving the steel, q_{int}, to enter the mold. To calculate this at every position down the mold, the model evaluates an effective heat transfer coefficient, h_{gap}, between the surface temperatures of the steel shell, T_s, and the hot face of the mold wall, T_{hotc}:

$$q_{int} = h_{gap} (T_s - T_{hotc}) \quad (6)$$

$$h_{gap} = \frac{1}{\left(\frac{d_a}{k_a} + \frac{d_f}{k_f} + \frac{d_l}{k_l} + \frac{d_{oeff}}{k_{oeff}} \right)} + h_{rad}$$

Heat conduction depends on the thermal resistances of four different layers. These depend on the time-averaged thickness profiles down the mold of the air gap, d_a, solid flux layer, d_f, liquid flux layer, d_l, oscillation marks, d_{oeff}, and their corresponding thermal conductivities. The most important resistances are usually the flux layers, whose thicknesses are calculated as described in the next section.

The equivalent air gap, d_a, is specified as input data and includes contact resistances at the flux / shell and flux / mold interfaces. It may also include a gap due to shrinkage of the steel shell, which is calculated using a separate thermal-stress model. [23] The shrinkage gap is affected by the mold taper and also by mold distortion, which can be calculated by another model.[Thomas, 1991 #89] This gap is important when simulating down positions near the corner.

Non-uniformities in the flatness of the shell surface are incorporated into the model through the prescribed average depth, d_{mark}, and width, L_{mark}, of the oscillation marks, as pictured in Figure 10. The oscillation marks affect the thermal resistance in two different ways. Firstly, they reduce heat conduction by providing an extra gap, represented by the effective average depth of the marks, d_{oeff}:

$$d_{oeff} = \frac{0.5\, L_{mark}\, d_{mark}}{(L_{pitch}-L_{mark})\left(1 + 0.5\, \frac{d_{mark}}{k_{mark}} \frac{1}{\frac{d_l}{k_l}+\frac{d_f}{k_f}}\right) + L_{mark}} \qquad (7)$$

where L_{pitch} is the ratio of the casting speed to the oscillation frequency, freq. This gap is assumed to be filled with either flux or air, depending on the local shell temperature. Secondly, the oscillation marks consume mold flux, so affect the behavior of the flux layer thicknesses, as described in the next section.

When the gap is large, significant heat is transferred by radiation across the semi-transparent flux layer.

$$h_{rad} = \frac{m^2\, \sigma\, (T_s^2 + T_{hotc}^2)(T_s + T_{hotc})}{0.75\, a\, (d_l + d_f) + \frac{1}{\varepsilon_s} + \frac{1}{\varepsilon_m} - 1} \qquad (8)$$

This depends on the absorption, a, and refractive index, m, of the powder, and emissivities of the steel and mold surfaces, ε_s and ε_m.

Below the mold, heat flux is applied as a function of spray cooling practice (based on water flux), natural convection, and heat conduction to the rolls. This enables the model to simulate the entire continuous casting process, if desired.

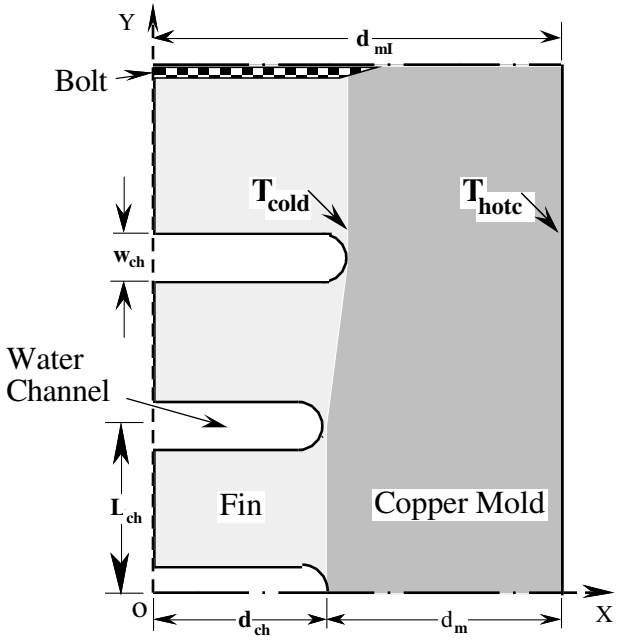

Figure 9 - Horizontal section through mold

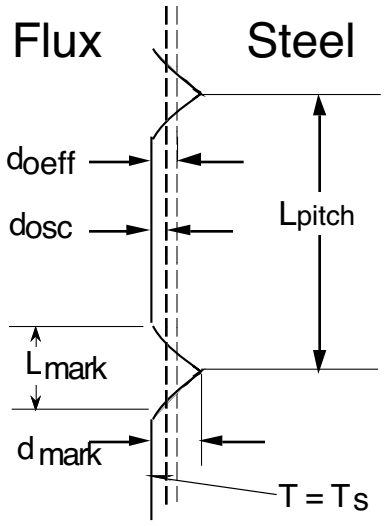

Figure 10 - Model treatment of oscillation marks

Flux is assumed to flow down the gap as two distinct layers: solid and liquid. The solid layer is assumed to move at a steady velocity, V_f, which is always greater than zero and less than the casting speed, V_c, according to the input factor, f_f.

$$V_f = f_f V_c \qquad (0 < f_f < 1) \qquad (9)$$

Velocity across the liquid layer is governed by the simple force balance:

$$\frac{\partial}{\partial x} \mu \frac{\partial v_z}{\partial x} = (\rho - \rho_{flux})\, g \qquad (10)$$

where a small body force opposing flow down the wide face is created by the difference between the ferrostatic pressure from the liquid steel, ρ g, and the average weight of the flux, ρ_{flux} g.

The casting speed is imposed at the point of contact between the shell and the liquid layer, which is assumed to flow in a laminar manner, owing to its high viscosity. The viscosity of the molten flux, μ, is assumed to vary exponentially with distance across the gap, according to the temperature:

$$\mu = \mu_o \left(\frac{T_o - T_{fsol}}{T - T_{fsol}} \right)^n \qquad (11)$$

where T_{fsol} is the solidification temperature of the flux, μ_o is the flux viscosity measured at reference temperature, T_o, (usually 1300 ˚C), and the exponent, n, is an empirical constant chosen to fit the measured data.

Equations 9-11 yield a velocity distribution across the flux layers, which is illustrated in Figure 11. Integrating across the liquid region yields an average velocity for the liquid layer, V_l:

$$V_l = \frac{V_c + V_f\,(n+1)}{n+2} + \frac{(\rho - \rho_{flux})\, g\, d_l^2}{\mu(T_s')\,(n+2)^2\,(n+3)} \qquad (12)$$

Mass balance was imposed to express the fact that the known powder consumption, Q_{flux} (kg m^{-2}), controls the total powder flow rate past every location down the interfacial gap. Flux can be carried by the solid layer, the liquid layer, or in the oscillations marks:

$$\frac{Q_{flux}\, V_c}{\rho_{flux}} = V_f\, d_f + V_l\, d_l + V_c\, d_{osc} \qquad (13)$$

The average depth of the oscillation marks (regarding their volume to carry flux), d_{osc}, is calculated assuming a V shape:

$$d_{osc} = \frac{0.5\, L_{mark}\, d_{mark}}{L_{pitch}} \qquad (14)$$

Two different regions can be distinguished down the mold, according to the lubrication condition. Close to the meniscus, the first region includes a liquid flux layer, which remains present so long as T_s‘ exceeds T_{fsol}. The liquid layer thickness is calculated by assuming a linear temperature profile across each layer in the gap (see Figure 11).

Flux in the oscillation marks remains liquid longer, due to the higher local shell temperature at their roots, T_s. Once the oscillation marks cool below the flux solidification temperature, however, the flux entrapped in them solidifies. This defines the second region, which consists of

totally solid flux, moving downward at the uniform speed, V_f. The oscillation marks no longer transport flux, so become filled with air.

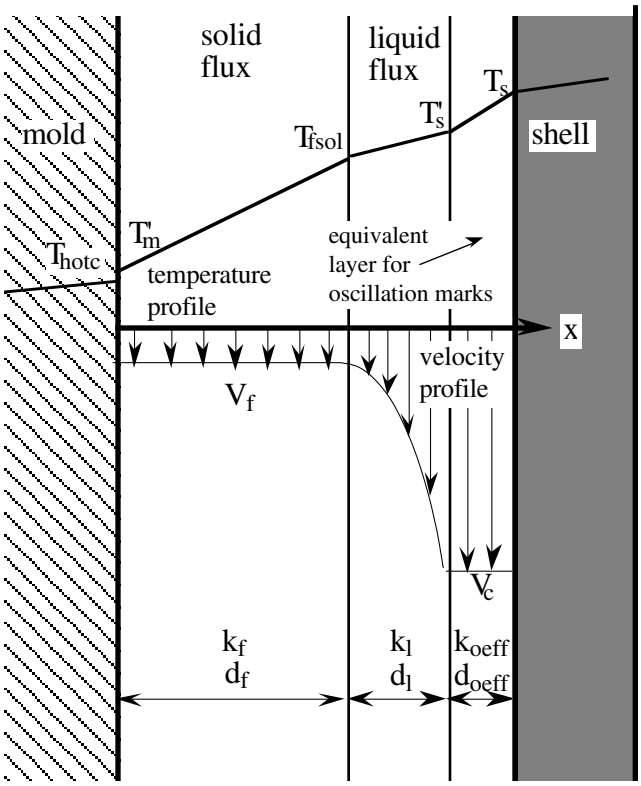

Figure 11 - Velocity and temperature profiles across interfacial gap layers (no air gap)

Solution Methodology

The CON1D model requires simultaneous solution of three different systems of equations: 1-D transient heat conduction and solidification of the steel shell, 2-D steady state heat conduction in the mold, and the equations balancing heat, mass and momentum in the gap. The equations are solved by first performing a transient 1-D simulation of the shell, gap and mold. The model uses an explicit, central-finite difference algorithm, which limits the maximum time step size, Δt. The results are used as initial conditions for the 2-D mold calculation, which is solved analytically by superposition, relating distance down the mold, z, to time in the shell through the casting speed. Subsequently, the model iterates between the 1-D shell and 2-D mold calculations using successive substitution until convergence is achieved. This produces a self-consistent prediction, which is stable for all coupled simulations investigated and converges in 3-4 iterations.

The model has been incorporated into a user-friendly FORTRAN program, CON1D. The program requires less than 500 KBytes of memory and runs on a personal computer in less than 1 minute.

Model Verification and Calibration

The model was first validated through comparison with known analytical solutions for metal-controlled solidification, [24] and with other models, which is described elsewhere. [25] It was then calibrated to match experimental measurements obtained under similar conditions to the breakout shell described in the previous section. These measurements included the cooling water temperature rise, the time-average temperature of several thermocouples embedded in the copper mold walls, and the thickness profile of the breakout shells. This calibration step is crucial because so many of the model parameters are uncertain.

Calibration was performed along the center of the wide face. Calibration is simplified here because there is no large air gap, such as found near the corners. This is because ferrostatic pressure pushes the long, wide, weak shell against the mold wide face to maintain as close a contact as possible.

The input parameters used in the simulations are given in Table I. Many of these parameters were measured (left side of table) while others are estimates of physical constants. The remaining parameters were adjusted to calibrate the model. These include the velocity of the solid flux layer, f_f, air gaps, and the thermal conductivity of the mold flux layers. Several other sets of calibrated parameters could have been chosen with equal matching of the measurements.

Table I Simulation Conditions and Parameters

	Slab breakout	Bloom	Model Parameters	
Mold specifications			d_a	0. - 0.025 mm
Slab size (z=0)	1500 x 225 mm	650 x 413 mm	k_{air}	0.06 $Wm^{-1}K^{-1}$
Mold Length	900 mm	900 mm	k_m	315 W $m^{-1}K^{-1}$
Working mold length	815 mm	775 mm	T_{water}	30 ˚C
Mold thickness $d_m(0)$	57 mm	15 mm	ρ_{flux}	2500 kg m^{-3}
Channel L_{ch}, d_{ch}, w_{ch}	24, 25, 5 mm	plate mold	T_{fsol}	980˚C
Mold curvature radius	11.76 m		μ_o	1.28 Poise
Water velocity, V_W	7.8 m s^{-1}		T_o	1300 ˚C
			n	0.85
Steel Composition	0.044%C	0.055 %C	k_f	1.24 $Wm^{-1}K^{-1}$
Liquidus, T_{liq}	1528 ˚C	1527 ˚C	k_l	3.4 $Wm^{-1}K^{-1}$
Solidus, T_{sol}	1509 ˚C	1500 ˚C	k_{scale}	0.55 $Wm^{-1}K^{-1}$
			d_{scale}	0.01 mm
Casting Conditions			σ	$5.67x10^{-8}$ $Wm^{-2}K^{-4}$
Casting speed, V_c	1.016 m min^{-1}	0.5 m min^{-1}	a	900 m^{-1}
Initial temperature, T_o	1555 ˚C	1546 ˚C	m	1.5
Superheat, ΔT_{sh}	27 ˚C	19 ˚C	ε_s, ε_m	0.8, 0.5
Consumption, Q_{flux}	0.4 kg m^{-2}		f_f	16.4 pct
			f_{sol}	70 pct
Oscillation Data			g	9.8 m s^{-2}
Stroke	10 mm		ρ	7400 kg m^{-3}
Frequency, freq	1.417 Hz		ΔH_L	272 kJ kg^{-1}
Average depth, d_{mark}	0.33 mm		L_{pitch}	12 mm
Average width, L_{mark}	3.78 mm		Δt	0.0005 s
Pitch (measured)	10.5 mm		Δx	0.3 mm

Mold Cooling Water Temperature Rise

The measured average rate of heat flux extracted from the mold should match that calculated by the model via:

$$Q\ (kW/m^2) = \frac{V_c}{z_{mold}} \sum_{mold} q_{int} * \Delta t \qquad (15)$$

This heat transfer rate is readily inferred from the temperature increase of the mold cooling water, ΔT_{water}, which is also calculated:

$$\Delta T_{water} = \sum_{mold} \frac{q_{int}\, L_{ch}\, V_c\, \Delta t}{\rho_w\, C_{pw}\, V_w\, w_{ch}\, d_{ch}} \qquad (16)$$

where ρ_w, C_{pw}, and V_w are the cooling water density, specific heat, and speed. This equation assumes that the cooling water slots have uniform rectangular dimensions, w_{ch} and d_{ch}, and spacing, L_{ch}. Heat entering the hot face (between two water channels) is assumed to pass entirely through the mold to heat the water flowing through the cooling channels. The prediction must be modified to account for missing slots due to bolts or water slots which are beyond the slab width, so do not participate in heat extraction.

For the LTV mold, the predicted cooling water temperature rise of 8.9 ˚C matches the measured rise. The predicted mean heat flux of 1495 kW/m^2 is thus also consistent with measurements.

Mold Temperatures

Figure 12 shows an example comparison between the predicted and measured temperatures at several locations down the LTV mold. The conditions were very similar to those of the breakout in Table I. The differences, given in run 2 in Ho, [20] include V_c=1.07 m min^{-1}, ΔT_{sh}=21˚C, Q_{flux}=0.6 kg m^{-2}, and a flux rim at the meniscus. The agreement suggests that the model is reasonably calibrated for typical casting conditions for this caster. This figure also shows the predicted hot face and cold face temperature profiles. The sudden changes in temperature are due to a 6.35 mm increase in water channel depth in the upper 300 mm of this test mold.

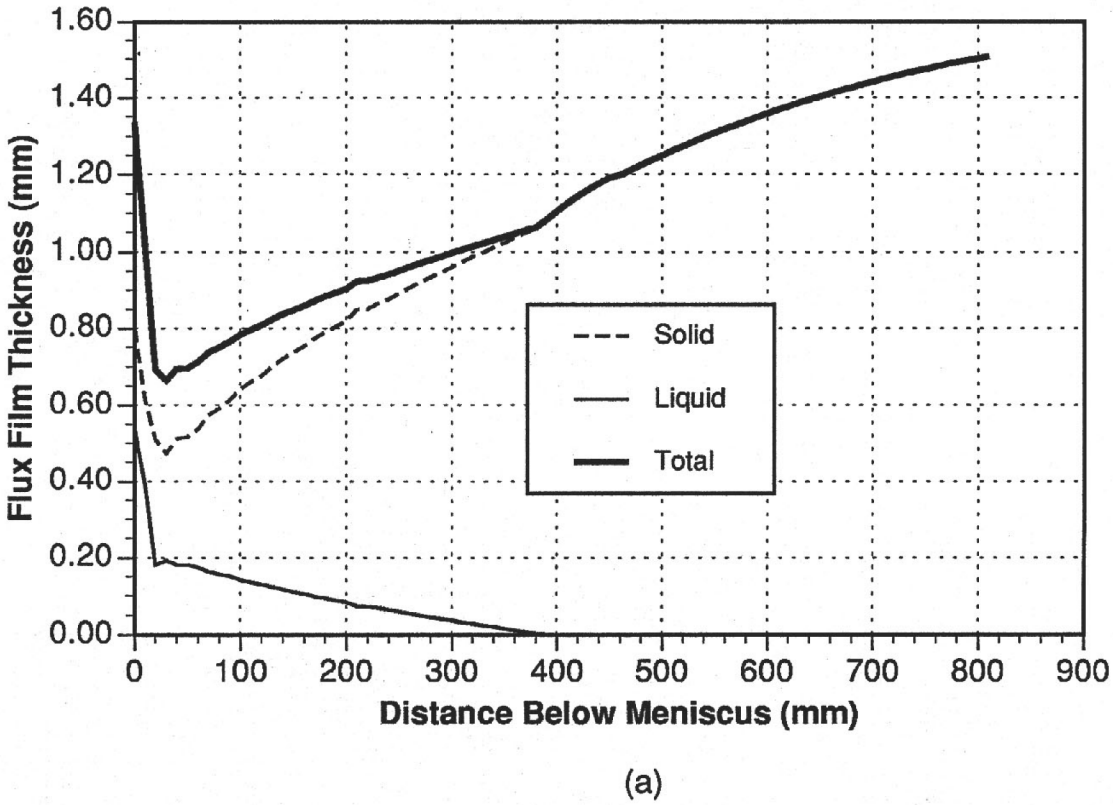

Figure 12 - Comparison between CON1D calculated and measured mold temperatures

Shell Thickness

Figure 4 includes a comparison of the predicted shell thickness profile with measurements down the breakout shell. Shell thickness is defined in the model by linearly interpolating the position between the liquidus and solidus isotherms corresponding to the specified solid fraction, f_{sol}.

Growth of the shell naturally depends upon the combination of the interfacial and superheat fluxes. The superheat distribution is important as Figure 8 shows that the two heat flux curves are of the same magnitude in the lower regions of the mold near the narrow face where the hot

molten steel jet impinges against the solidifying shell. The model is seen to match the measurements reasonably well.

Other Validation

The model predicts the thickness and velocity profiles expected in the powder layers in the interfacial gap. For example, Figure 13 shows the solid and liquid flux layer thickness profiles expected for the conditions in Figure 12 (Table 1). Unfortunately, no reliable samples could be obtained to validate these results, although the predictions of flux layer thickness on the order of 1 mm are consistent with findings at other plants. [20] Also, mold friction measurements should correlate with the model predictions of the length of the liquid layer, if data were available. Finally, model predictions of surface temperature of the steel shell could be compared with measurements from optical pyrometers located just below mold exit.

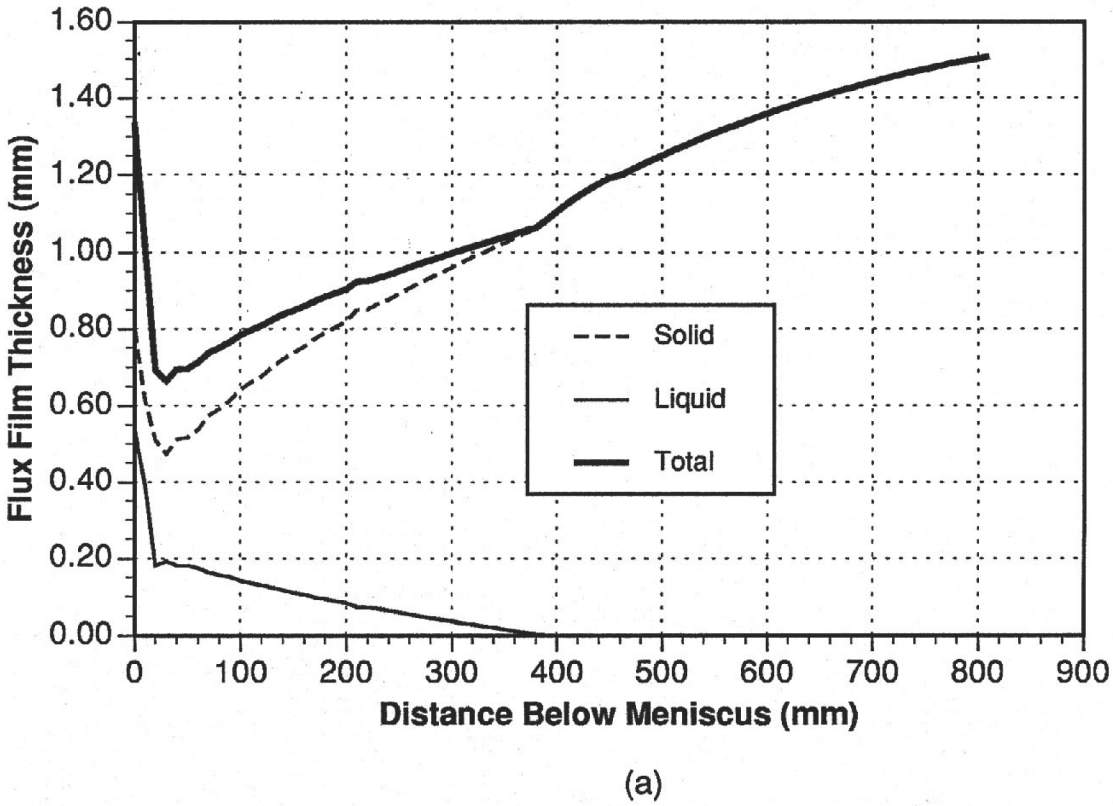

Figure 13 - Calculated flux layer thickness profile

CON1D model results

The calibrated CON1D model was run to perform a parametric study on the effect of the average oscillation mark area on the time-averaged heat transfer and shell growth. The average interfacial heat transfer coefficient, h_{gap}, was decreased by increasing the average effective depth of the oscillation marks, d_{oeff}, according to the average mark dimensions using Eqs. 6 and 7. Other parameters were left at their calibrated or measured values given in Table I.

For a fair comparison, the mold flux consumption rate for each run, Q_{flux}^{i}, was changed according to the oscillation mark area, assuming that oscillation marks with larger volumes consume more flux as they move downward at the casting speed:

$$Q_{flux}^{i} = Q_{flux} + \rho_{flux} (d_{osc}^{i} - d_{osc}) \quad (17)$$

Table II shows the conditions assumed and results for a typical case, based on Table I conditions, and extreme cases of no oscillation marks and very deep oscillation marks. The increased volume of the deeper oscillation marks is predicted to significantly increase flux consumption, according to Eqs. 14 and 17. It is important to note that if the consumption rate was not adjusted in this manner, then increasing oscillation mark depth would decrease the average gap thickness and thereby tend to increase the average mold heat transfer and shell thickness.

Table II Effect of Oscillation Marks on Mold Heat Transfer

	No marks	Typical	Deep marks	Units
Oscillation marks				
Volume	0.	0.62	3.00	mm^2/cm
Dimensions, d_{mark} x L_{mark}	0. x 0.	0.33 x 3.78	0.70 x 8.6	mm x mm
Average layer thickness, d_{osc}	0.	0.052	0.251	mm
Flux consumption, Q_{flux}	0.27	0.40	0.90	kg m^{-2}
Heat transfer coefficient (local)				
Osc. mark eff., k_{oeff} / d_{oeff}	∞	85000	14000	$Wm^{-2}K^{-1}$
Radiation, h_{rad}	133	137	160	$Wm^{-2}K^{-1}$
Gap, h_{gap} (flux-filled)	1890	1859	1720	$Wm^{-2}K^{-1}$
Average mold heat flux, Q_{int}	1573	1493	1322	kW m^{-2}
Shell thickness at mold exit	23.4	23.0	21.4	mm
Surface temperature at mold exit	902	983	1068	˚C

The results in Table II predict that deep oscillation marks decrease overall mold heat transfer by roughly 15%, relative to that with no oscillation marks. The shell thickness decreases accordingly, although the percentage drop is only 8% at mold exit. This is because the reduced heat transfer also increases the surface temperature of the shell exiting the mold. The hotter shell contains more heat and is also softer and weaker.

The calculated effect of oscillation mark depth on average shell thickness is illustrated in Figure 14. Shell thickness data were normalized by dividing by the corresponding thickness obtained with no oscillation marks, which has the maximum average thickness for a given case. The oscillation mark size was characterized by the area of the oscillation marks per unit length down the strand surface (0.5 d_{mark} L_{mark} / L_{pitch}). This is consistent with the importance of depth, width, and distance between the oscillation marks on heat transfer, which is quantified in Eq. 7.

The results predict that shell thickness decreases with deeper, wider, and / or more frequent oscillation marks, as expected. The effect is greatest near the meniscus (eg. 200 mm data), where the interfacial gap is the most influential factor controlling heat flow. Further down the mold, the increased thermal resistance of the thicker solid shell makes the oscillation marks less important. Shallow, flux-filled oscillation marks have a minimal effect on heat transfer because their thermal resistance (d_{oeff} / k_{oeff}) is so small relative to the rest of the gap and the solid shell.

The shell thickness predictions are compared with a few measured points in Figure 14. These points are not easy to obtain because it is difficult to estimate the thickness that the shell would have attained at a given location without the oscillation marks present. Thus, measured data points was only obtained at locations that had locally abnormally deep marks, relative to adjacent regions which could be used for comparison. Considering the scatter and uncertainty, the agreement with the model prediction is reasonable. Increasing oscillation mark area per unit length down the strand surface tends to decrease the shell thickness.

If typical oscillation marks become filled with air sometime before mold exit, h_{gap} is predicted to decrease by almost 50% from 1859 to 946 $Wm^{-2}K^{-1}$. Clearly, the material filling the gap has a tremendous effect on mold heat transfer. Oscillation marks become much more important if they

pull away from the flux and fill with air. This is predicted to happen when the surface temperature of the steel drops below the solidification temperature of the flux. It also happens when mold flux is not present. This occurs, for example, when there is poor flux entrainment or with oil lubrication. Thus, there should be a greater influence of oscillation marks on heat transfer in billet casting. This explains the larger drop in heat flux observed in middle-carbon steels in billet casters, relative to slab casters. [26]

These time-averaged results suggest that large dips in mold temperature indicate either very deep flux filled depressions, or much shallower air gaps.

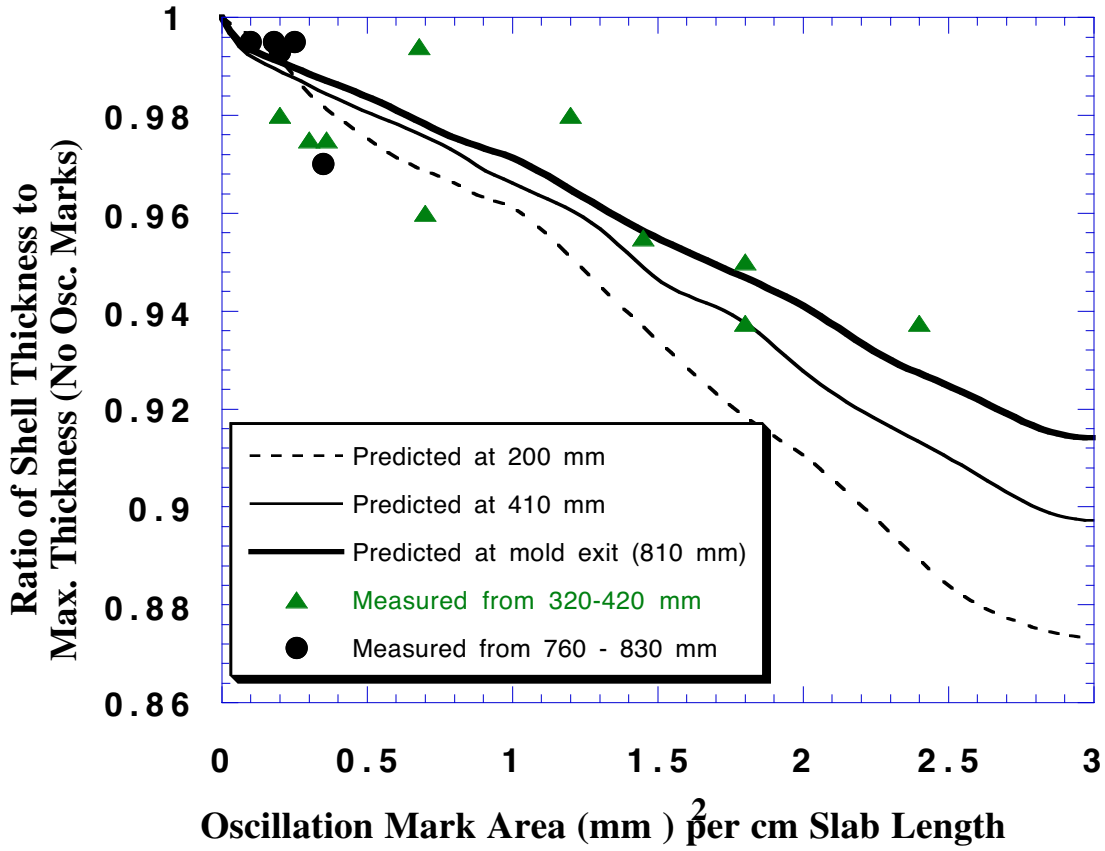

Figure 14 - Effect of oscillation mark area on normalized shell thickness

Two-Dimensional Model Description

A two-dimensional, transient model of the thermal-mechanical behavior of a transverse slice through the solidifying steel shell in a continuous slab casting mold has been developed and validated in previous work. [23] The model was applied here to investigate the effect of oscillation mark shape on transient interfacial heat transfer. Simulations were conducted to predict temperature evolution in small sections of the breakout shells, containing deep irregular oscillation marks. A 30 x 75 mm rectangular domain was chosen, starting at the meniscus with liquid at T_o. A steel shell solidifies on the left side of the domain as it moves down the mold at the casting speed. The other three sides of the domain are insulated.

The interfacial heat transfer coefficient, h_{gap} in Eq. 6, was varied with distance along the strand surface according to the local profile of the measured oscillation mark depth. Parameters defining h_{gap}, such as the thickness of the solid and liquid flux layers, were chosen to match the results from the calibrated CON1D model. [18] Typical results from the model are included in Figure 15, which shows the predicted isotherms in the rectangular domain at 23.6 s. [18] In order to compare with the breakout shell, time was related to distance below the meniscus knowing the casting speed and accounting for the extra solidification that occurred while the shell was draining through the breakout hole. [23]

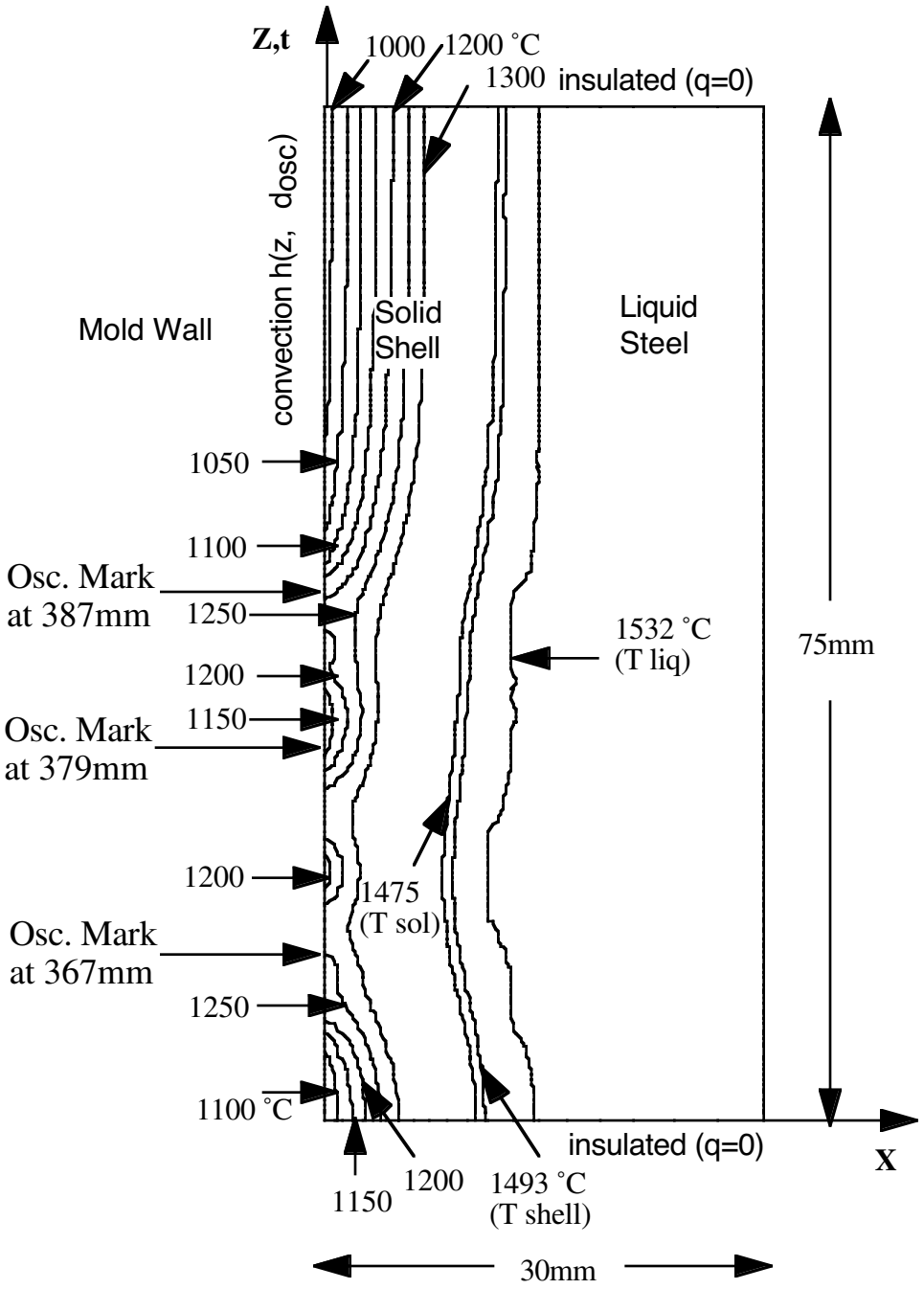

Figure 15 - Example 2-D heat flow model temperature distribution in shell section (with air-filled gap).

Two-Dimensional Transient Results

The CON1D model has quantified the effect of surface depressions on the steady-state heat transfer during continuous slab casting with mold flux. Next, the 2-D model is applied to investigate the local variations in heat transfer, shell growth, and surface temperature produced by individual groups of depressions on selected regions of the strand surface.

Shell thickness

Results for a section of shell with three typical oscillation marks (with areas of .34, .78, and 0.29 mm^2) are presented in Figure 16. The predicted shell thickness is compared with corresponding measurements of the breakout shell. The general agreement simply illustrates the reasonable calibration of the model, which was done for average oscillation marks similar to these (Table I).

Figure 16 also shows the measured surface profile for this section of shell, from which gap heat transfer coefficients were constructed using Eq. 6.

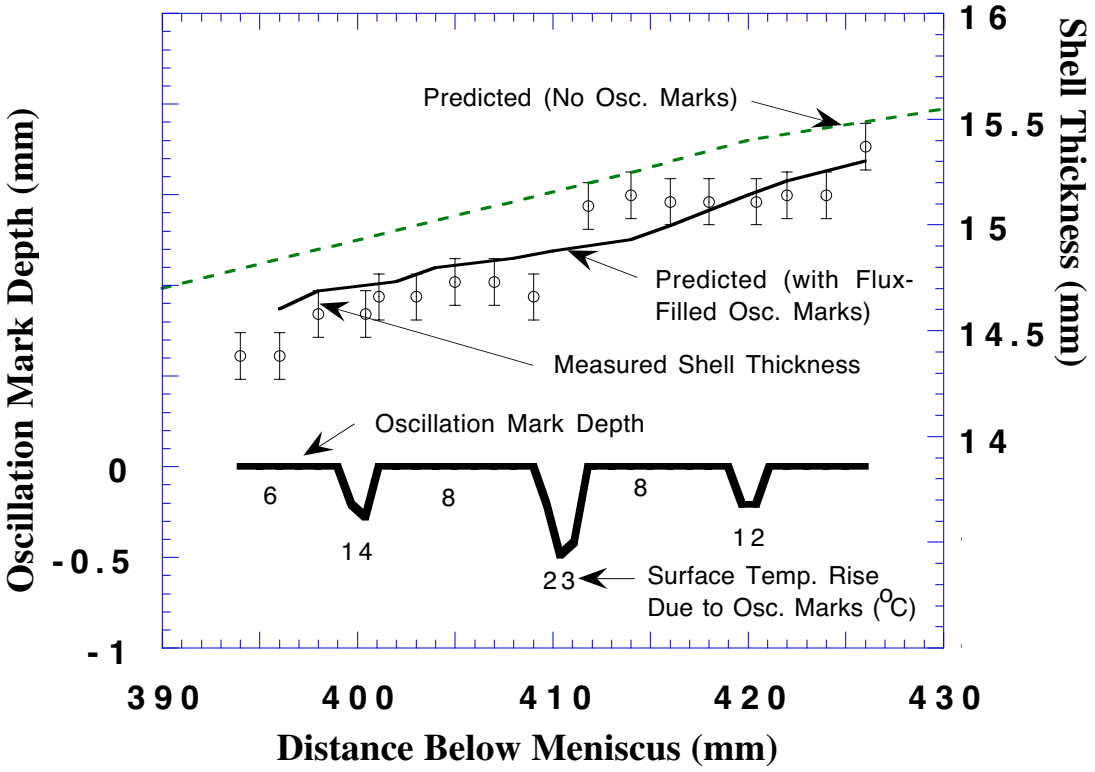

Figure 16 - Comparison of predicted and measured shell thickness with oscillation mark profile and surface temperatures for small, flux-filled oscillation marks

Each individual mark is almost too small to affect the shell thickness locally. The deepest (0.49 x 2.80 mm) middle mark in Figure 16 produces just a slight dip in shell thickness, which is enough to obscure the more important, general effect of reduced average shell growth rate. Without oscillation marks, the shell growth rate at 400 mm below the meniscus is predicted to be 0.021 mm per mm down the strand. These flux-filled oscillation marks produce a shell that is about 0.2 mm (1.5%) thinner.

Results from a section of shell with deeper surface depressions are shown in Figures 17 and 18. The four oscillation marks in this section of shell are seen to be very wide and deep, with areas of 1.8, 2.5, 1.9, and 1.1 mm^2. Even filled with flux, they significantly reduce the local shell growth. The decrease in shell thickness is predicted to range from 0.5 to 0.9 mm over this section (6% maximum loss). These predictions almost exactly match measurements from the breakout shell, as shown in Figure 17. This match is significant because the model calibration was performed for a different oscillation mark depth and did not consider local variations.

The maximum thickness loss is found midway along the section containing the four deep oscillation marks. Note that this does not coincide with the deepest oscillation mark. This is because these marks act as a group to reduce shell growth locally. Due to the nature of two-dimensional conduction within the shell, the number (or length) of the group of marks acting together is expected to roughly equal the local shell thickness. Thus, the group that controls growth at a particular point on the shell increases in number with distance down the mold. Near the meniscus, a single deep mark can produce a noticeable drop in shell thickness. By mold exit, however, only the effects of at least three oscillation marks extending over 30 mm can be distinguished.

To quantify the importance of the material filling the oscillation marks, the simulation of the deep oscillation mark section of shell was repeated using a lower thermal conductivity for the oscillation mark layer. Specifically, the material was changed from flux to air (Table I). The results in Figure 18 show the dramatic effect on heat transfer.

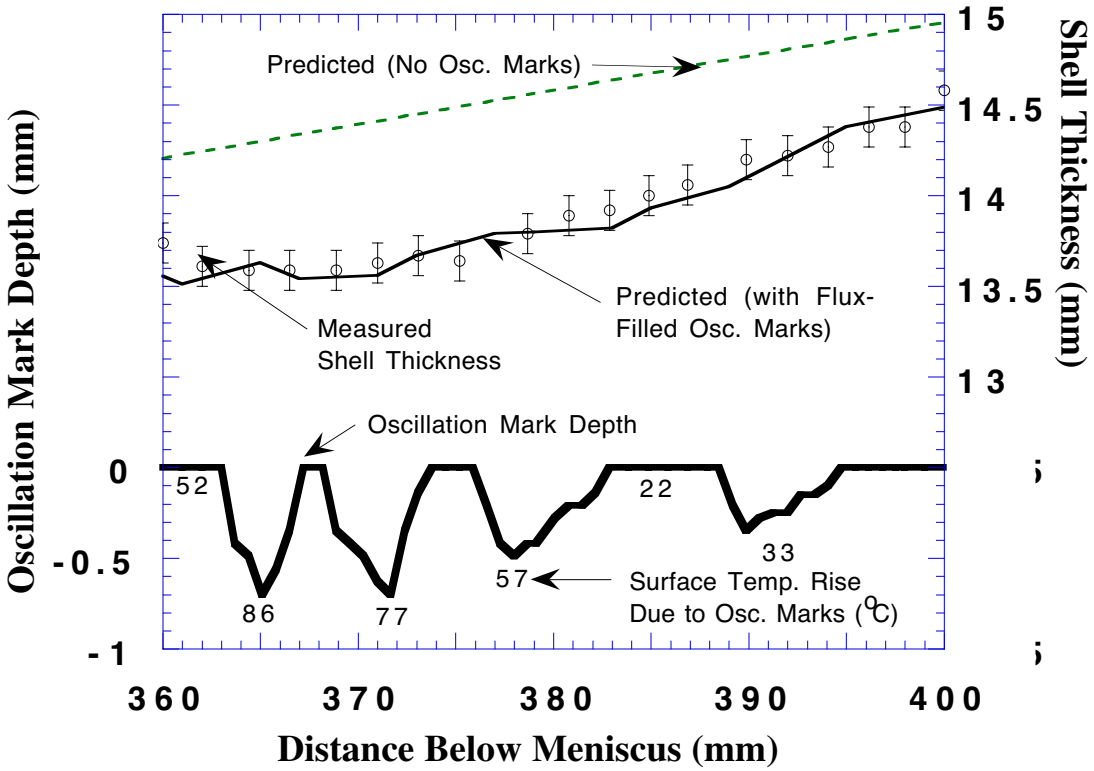

Figure 17 - Comparison of predicted and measured shell thickness with oscillation mark profile and surface temperatures for large, flux-filled oscillation marks

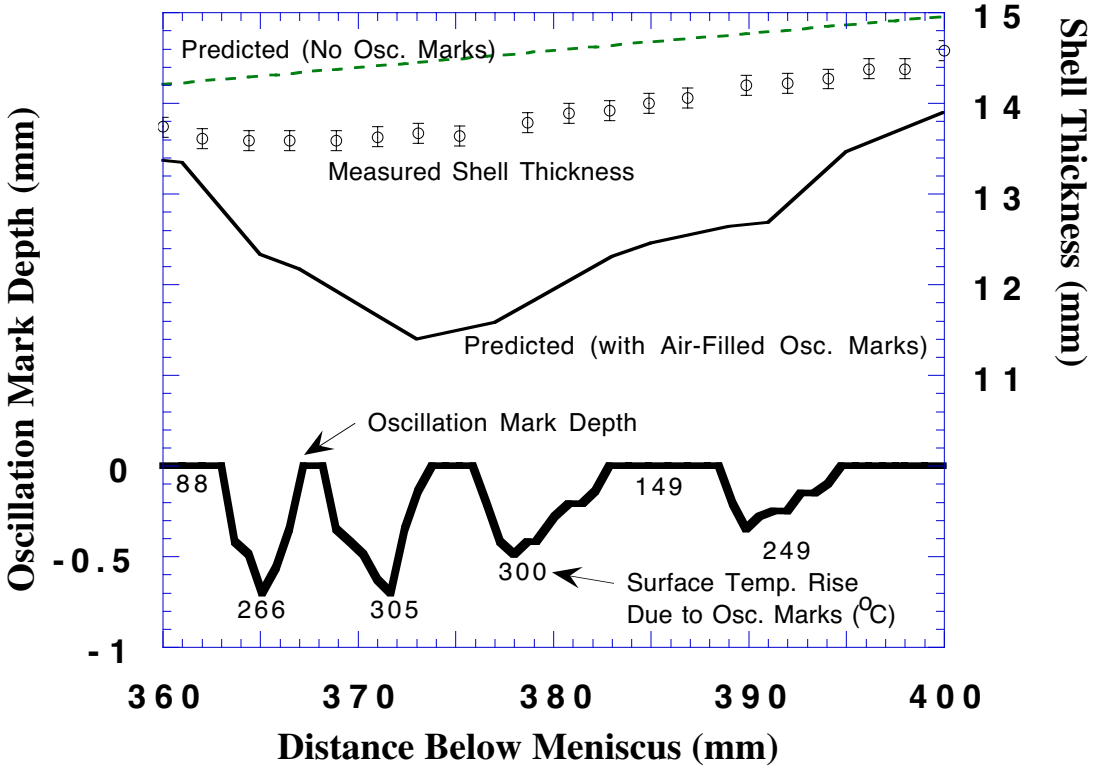

Figure 18 - Comparison of predicted and measured shell thickness with oscillation mark profile and surface temperatures for large, air-filled oscillation marks

The shell thickness is predicted to decrease by more than 3 mm (20%) in the region with air-filled oscillation marks. This does not match the measurements. This offers further proof that the oscillation marks in this investigation were not filled with air when they were in the mold.

Surface Temperature

Figures 16 - 18 also include the difference between the surface temperatures predicted with and without oscillation marks, labeled at significant locations along the shell. Surface temperature is more sensitive than shell thickness and corresponds directly with oscillation mark depth variations along the shell surface. Note that the oscillation marks increase the surface temperature even between the marks, where there is always a minimal gap between the shell and the mold. This is due to two-dimensional heat flow and further illustrates how several oscillation marks act together.

Small oscillation marks filled with flux increase temperature very little. At the root of a typical small (0.34 mm^2) oscillation mark in Figure 16, the temperature rise reaches only 14 ˚C. Such small variations are unlikely to produce any noticeable change in the mold temperature, relative to other parameters affecting heat flux, such as random changes in the flux layer thicknesses or gap properties.

Large oscillation marks filled with flux are predicted to produce significant rises in surface temperature of the strand. Figure 17 shows the surface temperature increases to 22 to 86 ˚C hotter than the 978˚C value predicted without oscillation marks. Like shell thickness, the extent of this variation decreases with distance down the mold. The changes in heat flux accompanying these temperature variations correspond to 20 to 50 ˚C fluctuations in mold temperature, depending on the location of the thermocouples. These temperature differences are typical of observed fluctuations in the recorded signals.

The temperature results in Figures 15 and 18 indicate the dangerous effect of air-filled surface depressions. The local surface temperature beneath a series of 2.0 mm^2 depressions filled with air rises more than 300 ˚C to nearly 1300 ˚C. The lower strength of the shell at this temperature, combined with its smaller thickness, would make the shell very weak locally and prone to failure. This simulation illustrates how deep surface depressions, combined with a mold flux entrainment problem that leads to deep air-filled depressions, could produce serious problems, such as a breakout. Large temperature differences between adjacent regions of the shell surface might also lead to crack formation. Finally, the large fluctuations in heat flux that accompany these temperature differences could be detected by the large fluctuations in the mold temperature signals they produce.

Discussion

Surface depressions, including oscillation marks, decrease heat transfer during continuous casting in the mold. This is manifested by drops in mold wall temperature, increased shell surface temperature and reduced shell thickness. The magnitude of these effects is proportional to the drop in heat transfer, which depends on the depth, width, and number of surface depressions per unit length along the shell, and the material that fills them.

Some of the temperature fluctuations recorded by thermocouples in the mold wall are clearly due to anomolously large depressions on the strand surface moving down the mold at the casting speed. These can be identified by a consistent time lag between dips recorded by thermocouples spaced vertically down the mold. The time lag corresponds to the casting speed and distance between thermocouples, as shown in Figure 2. Groups of oscillation marks with a similar large area are predicted to create a similar effect.

Oscillation marks likely have a greater importance in billet heat transfer, because the interfacial gap with vapor products from oil-based lubrication has such a low thermal conductivity. In flux-based casting operations, this work has shown that some, if not most, surface depressions are always filled with flux while in the mold. The impact of depressions on heat transfer under these good casting conditions is perhaps less than commonly thought, (only about 10% even for deep depressions).

The tremendous effect of air gaps suggests that problems in keeping the gap consistently filled with mold flux likely pose a greater threat to quality than the depth of the surface depressions. Future research should focus on the nature of the mold flux properties in filling the gap. Important factors to consider are the entrainment of flux at the meniscus, the loss of contact between the shell and the flux layers, and the break-up of the flux layer as it is dragged down the mold wall. Thus, flux properties such as coefficient of friction with the mold walls and tensile strength may be important and should be measured.

On-line quality monitoring systems should be developed to search for patterns in thermocouple signals and identify the likely presence of surface quality problems as they form in the mold. Corrective action can then be taken, and downgrading made as appropriate. Like shell surface temperature, mold thermocouple signals are more sensitive to changes in heat flux than is the shell thickness.

However, the use of thermocouple signals to detect defects is not easy. This is because 1) depressions do not always lead to defects and 2) many complex phenomena affect heat transfer, which are not related to depressions. For example, local increases in flux layer thickness and reductions in flux layer conductivity (eg. due to porosity) may lower gap heat transfer. These other factors, which have received little attention, are at least as important as surface depressions in controlling heat flux and thermocouple signals. [27] Thus, the lower heat transfer observed in middle-carbon steels is likely caused more by the higher solidification temperature mold fluxes (and accompanying thicker layers) employed for these grades, than to deeper oscillation marks.

Nevertheless, this work encourages on-line monitoring by showing how depressions affect the temperature history of the surface of the strand and can be detected by mold wall thermocouples. Further work is needed to determine the relationship between these thermal histories and defect formation.

Conclusions

Experimental measurements and calibrated solidification heat conduction models have been applied to understand the effect of surface depressions and oscillation marks on heat transfer and temperature in a continuous slab casting mold. Specific conclusions are:

1) Many surface defects, such as oscillation marks, originate at the meniscus and move down the mold at the casting speed. Their size and shape appears not to change over most of the length of the mold.

2) Surface depressions and oscillation marks reduce heat transfer, which slows shell growth, increases surface temperature, and causes dips in mold thermocouple signals. The magnitude of the effect depends on the size of the depression and the material filling it.

3) Shell thickness in the mold is reduced with increasing depth, width, and proximity of adjacent oscillation marks, which act together in groups. Typical flux-filled oscillation marks with 0.6 mm^2/cm produce a 1.5% drop in shell thickness. A group of 2 mm^2/cm marks produced a 6% decrease in shell thickness.

4) All of the oscillation marks and depressions investigated in this work were determined to be filled with mold flux.

5) The wideface off-corner region had the greatest variation in oscillation mark depth, which produced the greatest variation in local shell thickness.

6) Large (2 mm^2), air-filled depressions are predicted to drastically reduce heat transfer, slow shell growth by 20%, and increase surface temperature by 300 ˚C, which could lead to problems such as breakouts and cracks.

7) The effect of oscillation marks on heat transfer decreases with distance down the mold. They are most influential just below the meniscus, before the resistance of the solidified shell begins to control heat flow and lessen their importance.

8) Shell surface temperature and mold temperature are more sensitive to changes in heat flux caused by surface depressions than is the solidified shell thickness.

9) Large transverse surface depressions, or groups of deep oscillation marks can be positively identified by their characteristic effect on thermocouple signals as they move down the mold. Other phenomena occurring in the gap, such as the formation of air gaps, are also important to heat transfer and the accompanying fluctuations in thermocouple signals.

This work has taken initial steps to quantify the effect of imperfections in the cast surface shape on interfacial heat transfer. The findings should help improve the accuracy of model predictions of solidification heat transfer. In addition, they should be relevant to the interpretation of thermocouple signals for on-line quality monitoring.

Nomenclature

a	absorption coefficient (m^{-1})
C_p	Specific heat of steel (J kg^{-1} K^{-1})
d	Thickness in x direction (mm)
d_{mark}	Oscillation mark depth
d_{osc}	Effective mark thickness (volume)
d_{oeff}	Effective mark thickness (heat flow)
dscale	Scale layer on mold cold face
d_s	Steel shell thickness
f_f	Fraction V_c of solid flux speed
g	Gravity (9.81 m s^{-2})
h	Heat transfer coefficient (W m^{-2} K^{-1})
h_{rad}	Radiation across flux h
h_{fin}	Mold cold face h
h_{water}	Effective mold / water h
h_w	Mold surface / water h
h_{gap}	Shell / mold gap effective h
ΔH_L	Latent heat of fusion of steel (kJ kg^{-1})
k	Thermal conductivity (W m^{-1} K^{-1})
k_{oeff}	Effective k of osc. marks (W m^{-1} K^{-1})
K	Solidification constant ($mm^2 s^{-1}$)
L_{pitch}	Distance between osc. marks (mm)
L_{mark}	Width of oscillation marks (mm)
L_{ch}	Cooling water channel thickness (mm)
m	Refractive index
n	Flux viscosity exponent (Eq. 11)
q_{int}	Shell / mold interface heat flux (W m^{-2})
q_{sh}	Liquid / shell interface heat flux (W m^{-2})
Q_{flux}	Mold flux consumption (kg m^{-2})
t	Time (s)
Δt	Time step size (s)
T	Temperature (˚C)
T_{liq}	Liquidus temperature
T_{sol}	Solidus temperature
T_{fsol}	Solidification temperature of flux
T_{hotc}	Mold surface temperature
T_{water}	Mold cooling water temperature
T_s	Steel surface temperature
T_o	Reference temperature for μ
ΔT_{sh}	Superheat (T_{liq} - T_{sol})
V_c	Casting speed (m min^{-1})
V_f	Velocity of solid flux (mm s^{-1})
V_z	Casting direction velocity (mm s^{-1})
w_{ch}	Cooling water channel width (mm)
x	Shell thickness direction (mm)
Δx	Mesh spacing (mm)
y	Mold width direction (mm)
z	Casting direction (mm)
ε_s	Emmisitivity
ε_m	Mold emissivity
μ	Flux viscosity (T) (Poise)
μ_0	Flux viscosity at T_o (Poise)
ρ	Density of steel (kg m^{-3})
ρ_{flux}	Flux density (kg m^{-3})
σ	Stefan Boltzman constant

Subscripts

	solidifying steel shell (default)
water	mold cooling water
m	mold wall
a	air gap
flux	mold flux
f	solid mold flux layer
l	liquid mold flux layer
s	steel surface (oscillation mark root)
s'	steel surface

References

1. J.K. Brimacombe, "Empowerment with Knowledge - toward the Intelligent Mold for the Continuous Casting of Steel Billets," Metallurgical Transactions B, 24B (1993), 917-935.

2. W.H. Emling and S. Dawson, "Mold Instrumentation for Breakout Detection and Control," in Steelmaking Conference Proceedings, 74, Iron and Steel Society, Warrendale, PA, 1991), 197-217.

3. E. Takeuchi and J.K. Brimacombe, "The formation of oscillation marks in the continuous casting of steel slabs," Metallurgical Transactions B, 15B (Sept) (1984), 493-509.

4. B.G. Thomas and H. Zhu, "Thermal Distortion of Solidifying Shell Near Meniscus in Continuous Casting of Steel" (Paper presented at Solidification Science and Processing Conference, Honolulu, HI, 1995, JIM / TMS).

5. R.B. Mahapatra, J.K. Brimacombe and I.V. Samarasekera, "Mold Behavior and its Influence on Product Quality in the Continuous Casting of Slabs: Part II. Mold Heat Transfer, Mold Flux Behavior, Formation of Oscillation Marks, Longitudinal Off-corner Depressions, and Subsurface Cracks," Metallurgical Transactions B, 22B (December) (1991), 875-888.

6. J.E. Kelly et. al., "Initial Development of Thermal and Stress Fields in Continuously Cast Steel Billets," Metallurgical Transactions A, 19A (10) (1988), 2589-2602.

7. I.V. Samarasekera, J.K. Brimacombe and R. Bommaraju, "Mold Behavior and Solidification in the Continuous Casting of Steel Billets," Transactions of Iron and Steel Society, 5 (1984), 79-105.

8. I. Halliday, "Continuous casting at Barrow," J. Iron Steel Instit, 191 (1959), 121-163.

9. S.N. Singh and K.E. Blazek, "Heat Transfer and Skin Formation in a Continuous Casting Mold as a Function of Steel Carbon Content," in Open Hearth Proceedings, 57, (Warrendale, PA: Iron and Steel Society, 1974), 16-36.

10. K.E. Blazek, I.G. Saucedo and H.T. Tsai, "Investigation on mold heat transfer during continuous casting," in Steelmaking Proceedings, 71, Iron and Steel Society, Warrendale, PA, 1988), 411-421.

11. M. Wolf, "Investigation into the relationship between heat flux and shell growth in continuous casting moulds," Trans Iron Steel Instit Japan, 20 (1980), 710-717.

12. A. Grill, K. Sorimachi and J.K. Brimacombe, "Heat Flow, Gap Formation and Break-Outs in the Continuous Casting of Steel Slabs," Metallurgical Transactions, 7B (1976), 177-189.

13. N. Tiedje and E.W. Langer, "Metallographic examination of breakouts from a continuous billet caster," Scandinavian J. Metallurgy, 21 (1992), 211-217.

14. A.W. Cramb and F.J. Mannion, "The measurements of meniscus marks at Bethlehem Steel's Burns Harbor slab caster," in Steelmaking Proceedings, 68, (Warrendale, PA: Iron and Steel Society, 1985), 349-359.

15. B.G. Thomas, "Mathematical Modeling of the Continuous Slab Casting Mold, a State of the Art Review," in Mold Operation for Quality and Productivity, A. Cramb, eds., (Warrendale, PA: Iron and Steel Society, 1991), 69-82.

16. R. Bommaraju and E. Saad, "Mathematical modelling of lubrication capacity of mold fluxes," Steelmaking Conference Proceedings, 73 (1990), 281-296.

17. M.S. Jenkins et. al., "Investigation of Strand Surface Defects using Mold Instrumentation and Modelling," in Steelmaking Conference Proceedings, 77, (Warrendale, PA: Iron and Steel Society, 1994), 337-345.

18. D. Lui, "Effect of Oscillation Marks on Heat Transfer in the Continuous Casting Mold" (Masters Thesis, University of Illinois, 1995).

19. B.G. Thomas, B. Ho and G. Li, "CON1D User's Manual" (Report, University of Illinois, 1994).

20. B. Ho, "Characterization of Interfacial Heat Transfer in the Continuous Slab Casting Process" (Masters Thesis, University of Illinois at Urbana-Champaign, 1992).

21. X. Huang, B.G. Thomas and F.M. Najjar, "Modeling Superheat Removal during Continuous Casting of Steel Slabs," Metallurgical Transactions B, 23B (6) (1992), 339-356.

22. C.A. Sleicher and M.W. Rouse, 18 (1975), 677-683.

23. A. Moitra and B.G. Thomas, "Application of a Thermo-Mechanical Finite Element Model of Steel Shell Behavior in the Continuous Slab Casting Mold," in Steelmaking Conference Proceedings, 76, Iron and Steel Society, 1993), 657-667.

24. M.C. Flemings, Solidification Processing, (McGraw Hill, 1974), 17-19.

25. B.G. Thomas and B. Ho, "Spread Sheet Model of Continuous Casting," J. Engineering Industry, 118 (1) (1996), 37-44.

26. M.M. Wolf, "Mold Heat Transfer and Lubrication Control - Two Major Functions of Caster Productivity and Quality Assurance," in PTD Conference Proceedings, 13, (Warrendale, PA: Iron and Steel Society, 1995), 99-117.

27. M.R. Ozgu and B. Kocatulum, "Thermal Analysis of the Burns Harbor No. 2 Slab Caster Mold," in Steelmaking Conference Proceedings, 76, Iron and Steel Society, Warrendale, PA, 1993), 301-308.

Acknowledgments

Funding for this work was provided by the Continuous Casting Consortium at the University of Illinois (Allegheny Ludlum, AK Steel, Armco, BHP, Inland, LTV, Stollberg) The authors also wish to thank researchers at LTV Steel, (Cleveland, OH) for providing plant data and the National Center for Supercomputing Applications for computing time.